Influence of the freezing process upon fluoride binding to hemeproteins

An-Suei Yang* and Arthur S. Brill*‡
*Department of Physics and ‡Biophysics Program, University of Virginia, Charlottesville, Virginia 22901 USA

ABSTRACT Fluoride association with ferric myoglobins and hemoglobins in aqueous buffers above freezing has been well studied. We chose this reaction to investigate the feasibility of observing titration intermediates and estimating dissociation constants at the freezing temperature by electron paramagnetic resonance spectroscopy at cryogenic temperatures. Dependence of apparent dissociation constant upon protein concentration was observed, a factor of four decrease in protein accompanied by about a fourfold increase in the apparent tightness of binding in the range of protein concentration studied. Binding was also found to depend upon cooling rate and concentration of additives (serum albumin, sucrose, glycerol). These effects appear to be associated with freezing-induced concentration of ligand, a process described in the literature. Bands of high concentration of electrolyte accompany solute rejection during ice growth, sweeping by slowing moving macromolecules. Thus, just before being trapped in the solid, the protein can experience a greater concentration of salt than in the original liquid. A mathematical model of this process, based upon simplifying assumptions about nucleation and ice-crystal growth rates in super-cooled solution, shows how the average concentration of mobile solute species can depend upon the concentration of all species present. Semiquantitative computer simulations of the actual, more complex, freezing are also presented and lead to estimates of ice particle size which are then compared with estimates from the former model.

INTRODUCTION

The association of fluoride with ferric myoglobins and hemoglobins in aqueous buffers above freezing has been well studied (1–6). We chose this reaction to investigate the feasibility of observing titration intermediates and estimating dissociation constants at the freezing temperature by electron paramagnetic resonance (EPR) spectroscopy at cryogenic temperatures. A strong dependence of the apparent dissociation constant upon protein concentration is reported here, a factor of four decrease in myoglobin or hemoglobin concentration (at monomer concentrations below 4 mM) being accompanied by about a fourfold increase in the apparent tightness of binding. (The reduction of free fluoride by the amount bound in the complex with heme has been taken into account.) The apparent dissociation constants measured by EPR spectroscopy at cryogenic temperatures are also dependent upon the cooling rate of the sample during the freezing process and the concentrations of additives (bovine serum albumin [BSA], sucrose, or glycerol). These experimental results can be explained by freezing-induced concentration of the ligand in the solution, a process which has been studied extensively (7–13) but, because of its complexity, has not yet been mathematically modeled. The process is of biological and medical importance because many investigations (e.g., 14–16, 52) indicate it to be responsible for freezing injury to living cells and tissues. Freezing-induced solvent-solute segregation is also a cause of artifactual line shapes in EPR spectra from small paramagnetic species, and effective elimination of this segregation in polydextran gels has been described (7, 11).

When, during the freezing process, ice crystals start to nucleate and grow in an aqueous protein solution, the homogenous liquid phase changes discontinuously into an inhomogeneous solidified phase. At the beginning of the process, spherulites of almost pure ice separate from the solution. At the end, concentrated acids and bases from the buffer system, and other mobile species, freeze at the eutectic point and are trapped in many small pockets between ice crystals (17). Water, on the surface and in channels or cavities of the protein macromolecule, remains unfrozen and forms glassy microstructures when the temperature drops further (18, 53). Kinetic aspects of the freezing process play important roles in determining the final state of the solid phase. A concentrated layer of solutes, expelled from a growing ice crystal, forms at the interface between ice and solution as this surface propagates during freezing (9, 10, 19). The interface can carry significant electric potential if the ice lattice favors, and hence incorporates preferen-

Dr. Yang's present address is Department of Biochemistry and Molecular Biophysics, College of Physicians and Surgeons of Columbia University, New York, NY 10032.

0006-3495/91/05/1050/14 $2.00

tially, an ionic species (20). Other properties of the ice-solution interface are determined by the size of the ice crystal and its growth rate, both of which are governed by the geometry and rate of heat conduction of the sample and by the physicochemical properties of the solutes (21–24).

Among the complex of features of the freezing process, this paper is focused upon the solute redistribution which occurs during freezing of protein solutions. Bands of increasing concentration of expelled solute accompany the growth of ice crystallites and sweep by the relatively slowly moving macromolecules. Thus, just before it is trapped in the solid phase, the protein can experience a much greater concentration of salt than was present in the original liquid sample (9). The mathematical model, based upon simplifying assumptions about ice nucleation and growth, presented in this paper quantifies influences of nucleation and growth rates upon ice particle size and, together with fluoride diffusion, upon the average concentration of ligand to which the protein is exposed as it encounters the ice-solution interface. Measurements of this average fluoride concentration by EPR spectroscopy, and of the time required for freezing by light transmission, are described here. Such measurements enable one to characterize the effects of added solutes upon ice formation. Computer simulations of the cooling process, based upon heat formation and conduction, are used to calculate the average dimension of ice particles as a function of the cooling rate. The mathematical model and computer simulations do not incorporate every detail of the freezing process quantitatively. Instead, they offer semi-quantitative insight into the effects of heat conduction rate and solvent composition, as well as the concentration of protein itself, on the inhomogeneous redistribution of ligand in the protein solution during the freezing process.

MATERIALS AND METHODS

Horse heart myoglobin was purchased from Sigma Chemical Co. (St. Louis, MO). Human and horse hemoglobins were prepared from red blood cells. Ferric hemoglobins (metHb) and ferric myoglobin (metMb) were prepared as described previously (25). The protein solutions were buffered by 0.033 M potassium and sodium (K/Na ≈ 5:2) phosphate at pH 6.3 (at 22°C). Bovine serum albumin (BSA), 98–99%, was obtained from Sigma Chemical Co., and was used without further treatment. All protein solutions were centrifuged to eliminate suspended particles.

The course of freezing of protein solutions in an EPR sample cell was monitored optically with the cell in the tail of Varian variable temperature dewar, as shown in Fig. 1. EPR measurements were carried out at 77 K with a Varian 4500 X-band spectrometer modified in its microwave bridge. The sample was rapidly immersed in liquid nitrogen in a quartz/pyrex dewar, the quartz tail of which was inserted into a Varian 4531 general-purpose cavity.

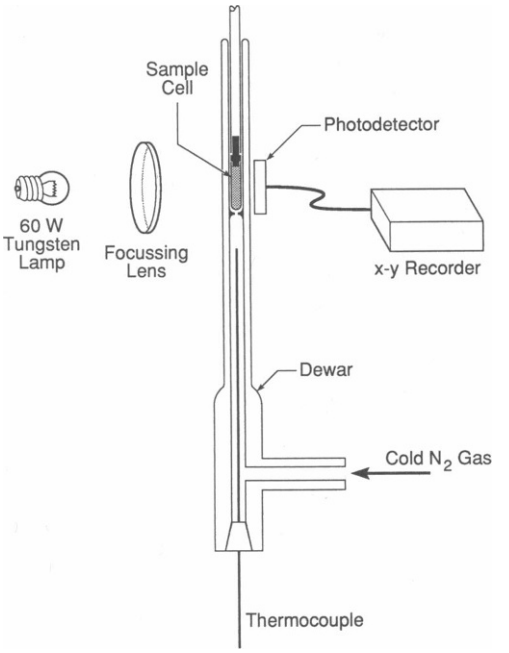

FIGURE 1 Apparatus used to monitor freezing of solution in EPR sample cell. Cold nitrogen gas (850 l/h) comes from a Varian device which controls the temperature with an electric heating element. The EPR sample cell is made of polyethylene. The temperature of the nitrogen gas is monitored by a copper-constantan thermocouple in the dewar. The temperature of the sample solution is measured by inserting the same type thermocouple of smaller diameter (0.13 mm) through the pin hole of the Teflon stopper and into the cell. A photoresistor (model MKB 7H38; Solar Systems, Inc., Skokie, IL) was employed for a detector.

The apparent dissociation constant of the fluoride complex of metMb or metHb, K_{ad}, is defined by the following equation.

$$K_{ad} = \{(1 - x)/x\}\,[F^-], \qquad (1)$$

where x is the mole fraction of the fluoride complex, obtained from the measured EPR spectra with the relation $x = \Delta h/\Delta h_0$, and $[F^-]$ is the (homogeneous) concentration of free fluoride after correction for amount bound in the complex. (After freezing, the distribution of fluoride is inhomogeneous, this inhomogeneity being responsible for the apparent increase in tightness of binding, i.e., decrease in K_{ad}, accompanying freezing.) Here the Δh values are differences between EPR (first derivative) signal amplitudes (at the field corresponding to the peak for the fluoride complex) when fluoride is present and absent, as shown in Fig. 2, where spectrum 1 is from 100% aquo complex and spectrum 12 from ~100% fluoride complex.

The EPR sample cells are made of either quartz (ID 2.7 mm, wall 0.5 mm, volume 0.050 ml) or polyethylene (ID 2.6 mm, wall 0.4 mm, volume 0.048 ml). A teflon stopper is used to plug the sample cell. A pin hole passed through the center of this stopper provides a path for excess solution when the stopper is inserted. A flange on the stopper insures reproducible depth of insertion and, thereby, a reproducible volume of sample solution. EPR measurements on a cell repeatedly

refilled with metHb solution show that the uncertainty in sample size for any one filling is ±1.2%.

RESULTS

A series of EPR spectra from horse metHb, titrated with various concentrations of KF and measured at 77 K, is shown in Fig. 2. Scatchard plots of the titrations with fluoride at several concentrations of metMb or metHb are shown in Figs. 3, *a* and *b*, where $\Delta h'$ is Δh normalized for differences in heme concentration. The strong dependence of K_{ad} (inversely proportional to the slope of the Scatchard plot) upon protein concentration is immediately apparent. This remarkable effect is plotted in Fig. 4 for horse methemoglobin and horse heart metmyglobin. Within the range of protein concentration (expressed as [heme]) shown, the two proteins are seen to behave much the same with respect to the dependence of the dissociation constant upon their concentration; a fourfold increase in protein concentration is accompanied by about a fourfold increase in K_{ad} in the concentration range shown. At this time, measurements have not yet been made with the heme proteins at greater concentrations. While the straight line fit shown describes the behavior of K_{ad} for the data at hand, one would not predict such a relation to continue to apply as the concentration of protein is increased; rather, as the following experiment with bovine serum albumin (BSA) suggests (Fig. 5 *a*), "saturation" will occur as the concentration of heme protein is continually increased.

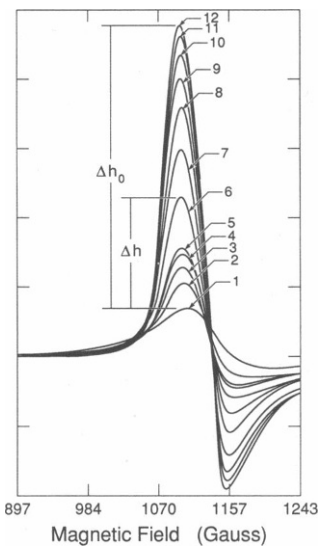

FIGURE 2 Titration of human methemoglobin with potassium fluoride. A quartz sample cell (ID 2.7 mm, wall 0.5 mm) was used to hold a constant volume (0.05 ml) of sample solution. The cell was immersed in a dewar of liquid nitrogen (T = 77 K), the tail of which was inside the resonant cavity. Sample solutions contained human methemoglobin, [heme] = 5.14 mM, in 33 mM phosphate, K/Na = 5:2, pH 6.3, buffer. The final concentrations (mM) of fluoride in these solutions were (1) 0, (2) 1.23, (3) 1.96, (4) 2.46, (5) 3.08, (6) 6.14, (7) 9.22, (8) 15.4, (9) 24.0, (10) 38.4, (11) 62.2, (12) 120. All spectra (first derivative) were taken with the same EPR instrument settings: microwave frequency, 9.30 GHz; microwave power, 36 mW; modulation frequency, 100 KHz; modulation amplitude, 6 G. The Δh values were measured at the magnetic field strength corresponding to the peak for the fluoride complex.

The possible effect of protein in general can be observed by adding an inert protein to the solution upon which measurements are being made. The result of such an experiment is shown in Fig. 5 *a*. With the heme protein concentration fixed at a low value, BSA is introduced at successively greater concentrations. K_{ad} is seen to increase linearly with [BSA] up to ~1 mM, in a manner analogous to (but somewhat more strongly than) the dependence of K_{ad} upon heme protein concentration. Above 1 mM the incremental effect of BSA diminishes, and K_{ad} has leveled off by the time [BSA] reaches 3 mM. Similarly the effects of adding solutes other than protein can be observed; thus far experiments with increasing concentrations of sucrose (Figs. 5 *b* and 7) and glycerol (Fig. 7) have been carried out and show that these additives influence K_{ad} in a manner similar to BSA but to different degrees. Clearly the mole fraction of hemeprotein complex formed in a frozen sample is influenced by the concentration and physicochemical properties of solutes or organic cosolvents in the protein solution. As will be shown below, the rate of freezing also affects the extent of fluoride complex formation.

The EPR spectra upon which Figs. 2–5 are based were measured with samples in a quartz cell. Both quartz and polyethylene (PE) cells were used in the experiments reported here. When the quartz cell, filled at room temperature with sample solution, is rapidly immersed in liquid nitrogen, a time of 14 s is required for the temperature at the center of the cell to drop to 100 K. With the PE cell, under the same experimental conditions only 6 s is required. While the properties of PE depend strongly upon how the plastic is manufactured, on the average the thermal conductivity of PE is ~3 times smaller than that of quartz at room temperature, and somewhat less than 2 times smaller at 120 K. On the basis of differences in thermal conductivity, the samples in PE cells should take longer to cool down than those in quartz cells. A likely explanation of the contrary phenomenon is in terms of differences in thermal expansion among the three materials involved; quartz is notable in its very small dimensional change with temperature, PE contracts greatly with cooling, and ice is between quartz

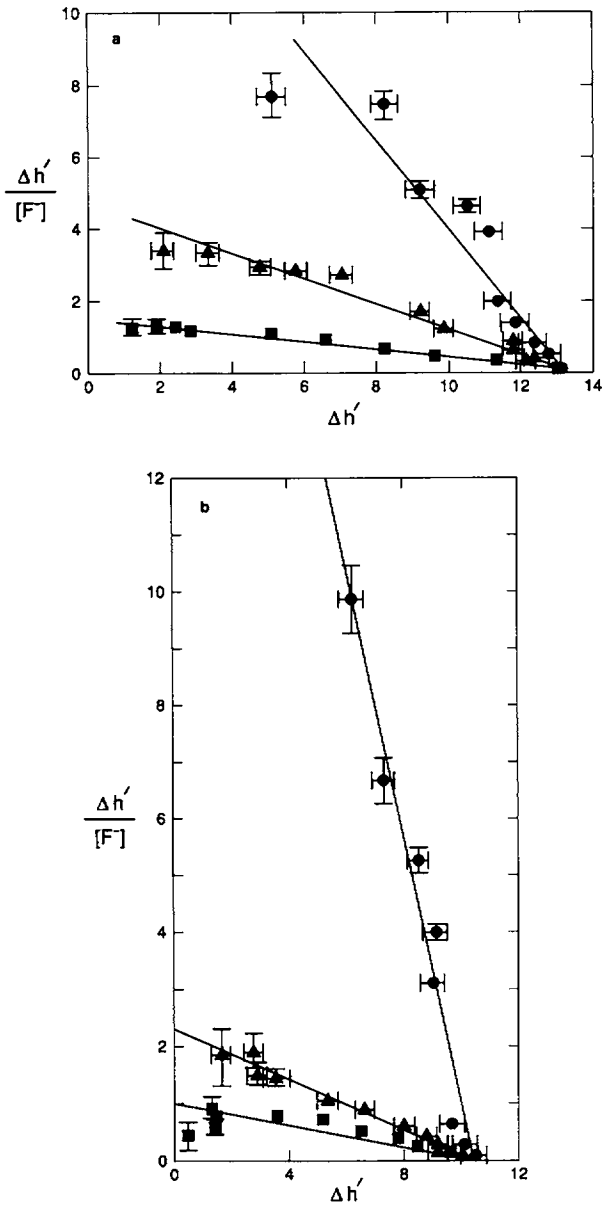

FIGURE 3 Scatchard plots for titrations of horse methemoglobin and horse heart metmyoglobin with potassium fluoride. $\Delta h'$ (x-axis) is the difference in EPR amplitude (measured at the field for the fluoride peak) between spectra from solutions containing fluoride and the spectrum from 100% aquo complex (see Fig. 2), divided by [heme]. $\Delta h'/[F^-]$ (y-axis) is this difference divided by the concentration of unbound fluoride. The slope of the Scatchard plot is $-1/K_{ad}$, where K_{ad} is the apparent dissociation constant of the hemeprotein-fluoride complex (see Eq. 1). The apparatus and experimental conditions were those of Fig. 2, except that the microwave power was set at 230 mW for the lowest concentrations of the two hemeproteins. No saturation of the EPR signals from either the aquo or fluoride complexes was found at the powers used. (*a*) Horse methemoglobin: [heme] = 0.183 mM, K_{ad} = 0.8 ± 0.3 mM (●); [heme] = 0.904 mM, K_{ad} = 2.9 ± 0.5 mM (▲); [heme] = 3.84 mM; K_{ad} = 8.8 ± .5 mM. (*b*) Horse heart metmyoglobin: [heme] = 0.179 mM, K_{ad} = 0.39 ± 0.07 mM (●); [heme] = 1.87 mM, K_{ad} = 4.8 ± 0.5 mM (▲); [heme] = 3.67 mM, K_{ad} = 11.5 ± 1 mM (■).

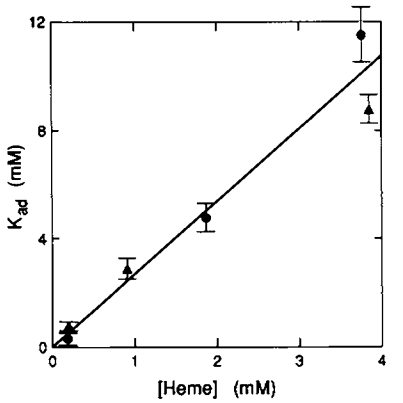

FIGURE 4 Dependence upon protein concentration (expressed as [heme]) of the apparent dissociation constant (K_{ad}) for the fluoride complexes of horse methemoglobin (▲) and horse heart metmyoglobin (●). The K_{ad} are from the Scatchard plots of Fig. 3.

and PE in this behavior. These differences in thermal expansion (contraction) suggest that the PE cell will shrink tightly on to a frozen aqueous sample within it, and that a frozen aqueous sample will shrink away from the walls of a quartz cell containing it, leaving a poorly conducting interface between. Because the PE cells were found to survive more freezing-thawing cycles (when filled with aqueous samples), they have supplanted the quartz cells for measurements at low temperatures and were used for the experiments (and simulations) of Figs. 6–13.

The rate of heat conduction from the sample influences the extent of hemeprotein-fluoride complex formation in frozen solutions. The mole fraction of fluoride complex was measured to be 0.6 at 77 K for a solution of metHb ([heme] = 0.245 mM) and KF (1.23 mM) in 0.033 M phosphate buffer, pH = 6.3, frozen by rapidly immersing the quartz cell containing it in liquid nitrogen. With the same solution in a polyethylene cell, and for the same procedure, the mole fraction was measured to be 0.3. A more detailed discussion of the effects of cooling rate will be given in the following sections.

The K_{ad} values given above are (apparent) dissociation constants measured at 77 K without correction for either the ligand-concentrating effect of the freezing process or the inaccessibility, below 200 K, of the heme site to ligand molecules at the surface of the protein molecule (26). Immersion of the sample cell in liquid nitrogen does not provide enough time for the hemeprotein to equilibrate with freeze-concentrated local fluoride before the temperature drops below 200 K and the binding of fluoride is quenched. However, subsequent warming above 200 K permits local equilibration of fluoride and heme to occur; at 250 K this process is complete within 5

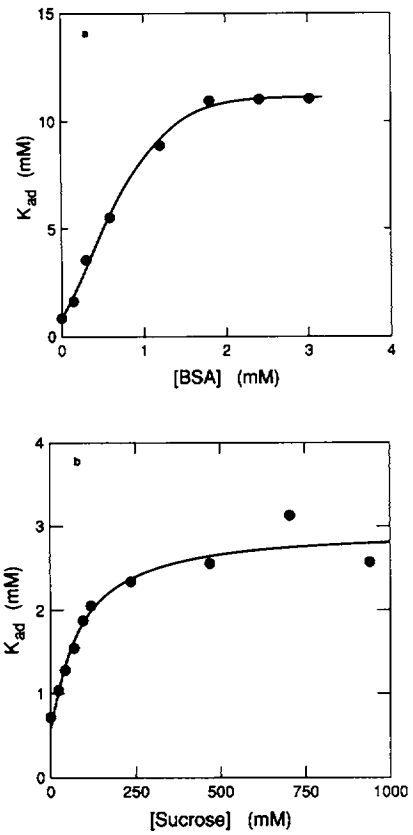

FIGURE 5 The effect of BSA (bovine serum albumin) and sucrose on the apparent dissociation constant of the human methemoglobin-fluoride complex. The apparatus and experimental conditions were the same as in Fig. 2, except that the power was set at 230 mW. The heme concentration was 0.245 mM throughout, and K_{ad} was estimated from the Δh produced by a single concentration, 1.23 mM, of potassium fluoride. (*a*) K_{ad} in the presence of various concentrations of BSA. (*b*) K_{ad} in the presence of various concentrations of sucrose.

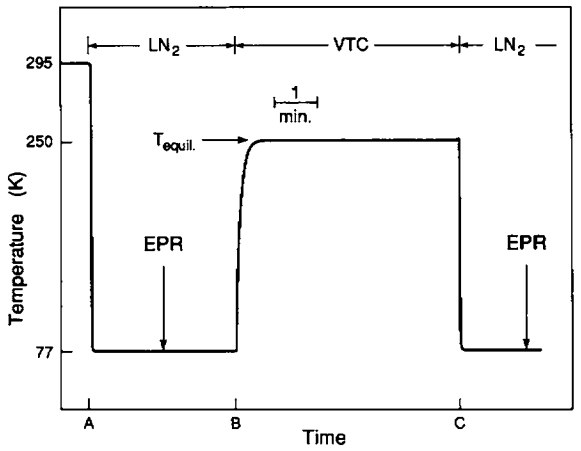

FIGURE 6 Sequence of temperature changes for measurements of ligand-heme equilibration after warming. The polyethylene sample cell is plunged into liquid nitrogen at *A*. At *B*, the sample cell is removed from the liquid nitrogen bath and inserted into the dewar of the variable temperature controller (VTC) with the temperature set at, e.g., 250 K. Five min later, at point *C*, the cell is plunged back into liquid nitrogen. EPR spectra were measured before and after the rewarming interval (*B-C*).

min (27). Fig. 6 depicts an experimental procedure for determining the apparent dissociation constants before and after equilibrium at temperature T. In Fig. 7 are plotted the mole fractions of fluoride complex in the presence of a range of concentrations of BSA, sucrose, or glycerol, before and after warming at 250 K. If the average local concentration $\langle C_0 \rangle$ of fluoride around the protein molecules in frozen solution were measurable, the intrinsic dissociation constant could be obtained from

$$K_d = \{(1 - x)\langle C_0 \rangle. \quad (2)$$

The presence of 27% (4.1 mM) BSA alters the freezing process in such a way that fluoride redistribution is effectively suppressed, and the average concentration of fluoride around the protein molecules is the same as that in the liquid solution above freezing. The intrinsic dissociation constant of the metHb-fluoride complex is then estimated from the Scatchard plot shown in Fig. 8 to be 12 ± 1 mM at 250 K.

The results of optical monitoring of the freezing of a

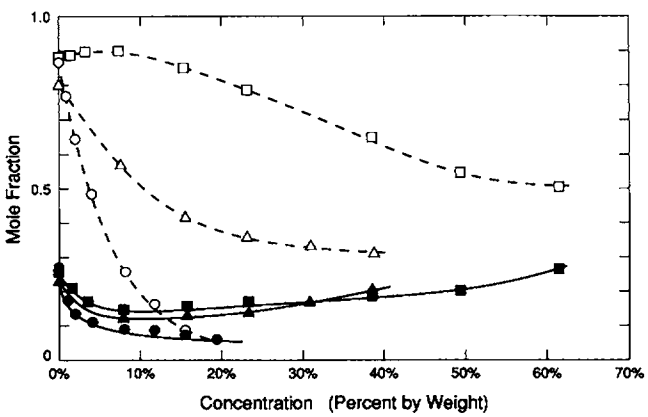

FIGURE 7 Warming-induced reequilibration of fluoride in the presence of various solutes. The data is from human methemoglobin, [heme] = 0.247 mM, in the presence of 1.18 mM KF. The mole fractions of fluoride complex, calculated from EPR spectra before (*solid lines and symbols*), and after (*dashed lines and open symbols*) warming at 250 K, are plotted as functions of the concentration (% by weight) of BSA (● and ○), sucrose (■ and □), and glycerol (▲ and △).

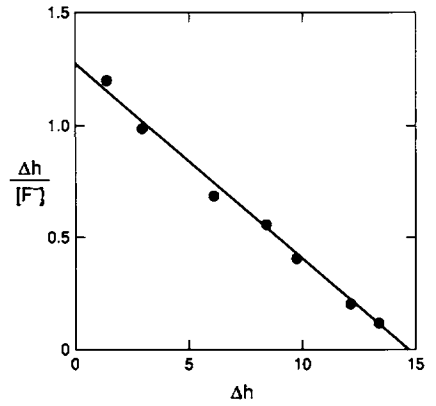

FIGURE 8 Scatchard plot of fluoride titration of human methemoglobin in the presence of 4.1 mM bovine serum albumin. A polyethylene cell was used to hold a sample of volume 0.048 ml, [heme] = 0.29 mM, buffer as in Fig. 2. The temperature sequence of Fig. 6 was employed with T_{equil} = 250 K. The linear least squares fit, shown as a solid line, has a negative inverse slope of 12 mM.

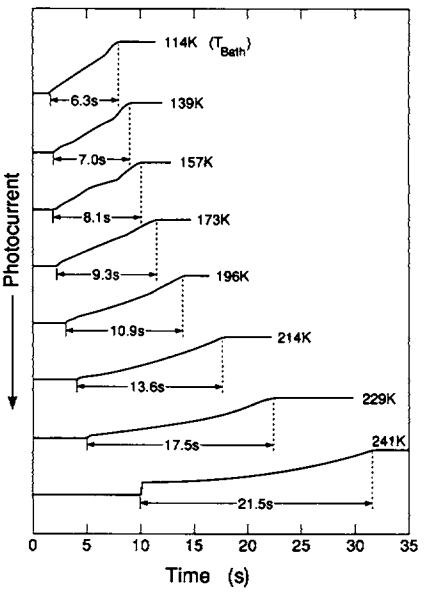

FIGURE 9 Measurement of t_0 of sample solutions frozen at eight bath temperatures between 114 and 241 K. A polyethylene cell (ID 2.6 mm, wall 0.4 mm, volume 0.048 ml) was filled with sample solution containing KF (1.18 mM) and human methemoglobin ([heme] = 0.247 mM) in 33 mM phosphate, pH 6.3, buffer. The sample cell was then bathed in cold nitrogen gas as shown in Fig. 1. t_0 is the period of time during which the optical transmission continuously changes. t_0 vs. bath temperature is also shown in Fig. 11 *c*. Within 5 s after the completion of freezing, the sample cell was rapidly immersed in liquid nitrogen and the EPR spectrum taken so that the mole fraction of fluoride complex could be calculated (see Fig. 11 *a*).

methemoglobin solution at eight bath temperatures are shown in Fig. 9. Measurements of this kind remain to be carried out on systematically varied protein solutions.

MODELS

It is well known that increasing the concentration of protein, sucrose, or glycerol, as well as rapid freezing, results in smaller ice crystals in frozen solutions (28–30). Once nucleation has started, the rate of formation of ice nuclei increases with decrease in the ratio of heat release (from ice nucleation and growth) to the rate of heat removal from the sample to the heat sink. Concentrated solute reduces the rate of ice growth (29), and lower temperature of the heat sink increases the rate of heat removal. Both effects reduce the ratio of the rate of heat release to heat removal, and, as a result, increase the concentration of nuclei which form per second. All our experiments indicate that a higher concentration of ice nuclei in a frozen sample, due either to more concentrated solute or to colder heat sink, results in a lower average concentration of fluoride to which the hemeproteins are exposed during freezing. We now describe a simple kinetic model and an adequately realistic computer simulation of the cooling and freezing process, based upon our and others' experiments. The model and simulation provide a basis for interpreting the relationship between the average concentration of fluoride around the hemeprotein molecules, and the average dimension of the ice bodies grown from each nucleus.

A. Simple kinetic model

Assume that, because of the small size of the sample and the fast rate of heat conduction from it, the temperature is approximately constant throughout the sample. When the temperature of the sample drops rapidly below the freezing point, spherulites (spherical ice bodies) grow uniformly from nuclei (21–24, 30). Each spherulite is made up of very small ice crystals. Most of the low molecular weight solutes are driven to the interface between solution and spherulite. Protein molecules are assumed to be largely trapped between the tiny ice crystals in the spherulites because of the low mobility of the macromolecules (9). Before being trapped in the frozen solid phase, the protein molecules are transiently exposed to a layer of concentrated solute (solute having been expelled from the ice during the growth of the spherulite). With a model based upon these ideas, the average concentration of fluoride around the protein molecules can be calculated as a function of both the nucleation and growth rates of ice.

Definitions and discussion of some parameters in this model are now given:

(*a*) r_s (cm): radius of a spherulite. In magnitude, $r_s < 0.1$ cm.

(*b*) R (cm^{-1}): rate of growth of a spherulite. On the basis of other observations (21), we take R to be constant throughout the growth of the spherulite and, hence, independent of r_s, provided the temperature is constant. In magnitude, $R \leq 0.01$ cm/s.

(*c*) v_n ($s^{-1}cm^{-3}$): nucleation rate of spherulites (ice nuclei per unit time per unit volume). v_n, a strongly temperature-dependent parameter, is in the range 10–10^4 $s^{-1}cm^{-3}$ for the freezing conditions of the experiments reported in this paper.

(*d*) $V(t)$ (cm^3): volume of liquid phase as function of time. $t = 0$ when nuclei start to develop, and $t = t_0$ when ice takes up all the volume. $V(0)$ is the total volume of the solution and $V(t_0) = 0$.

(*e*) D (cm^2/s): diffusion constant of ligand in the liquid phase at freezing temperature.

The availability of such diffusion constant data is limited. On the basis of values for other small ions in aqueous solution close to the freezing temperature, the diffusion constant for the fluoride ion is estimated to be between 10^{-6} and 10^{-5} cm^2/s, depending upon the freezing temperature and viscosity of the solution.

The treatment by Pohl (31) of solute redistribution for the case of zone melting, where recrystallization occurs at a planar interface, can readily be reformulated for a spherical interface. The corresponding concentration of fluoride as a function of distance from the nucleus of an ice spherulite is shown schematically in Fig. 10. C_0 is the distant ($r \gg r_s$) concentration of fluoride. The fluoride concentration on the spherical interface, C_s, is obtained from Eq. 27 of Pohl which gives solute concentration

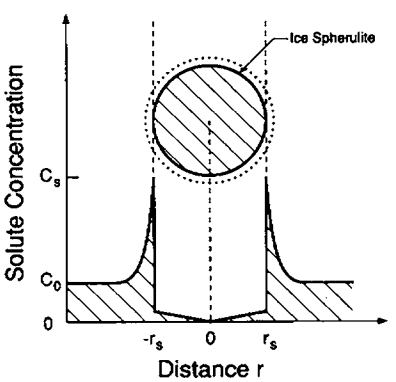

FIGURE 10 Schematic representation of ligand concentration as a function of distance from the nucleus of the spherulite. C_0 is the distant ligand concentration; C_s is the concentration of the ligand on the interfacial surface between spherulite and solution.

$c(x, \tau)$ as a function of distance (x) from the interface and time (τ):

$$C_s = c(x = 0, \tau = r_s/R) = C_0\{1 + [(1 - k)/k][1 - e^{-(1-k)(kR/D)r_s}]\}$$

which reduces to

$$C_s = C_0(1 + Rr_s/D) \text{ when } kRr_s/D \ll 1. \quad (3)$$

Here k is the equilibrium distribution constant of the solute between ice phase and solution ($k \equiv [\text{solute}]_{ice}/[\text{solute}]_{solution}$). k for sodium chloride is $< 10^{-3}$ (19, 32) and for hydrogen fluoride, $\sim 10^{-2}$ (34). Note that $r_s = R\tau$, a linear function of time, and that Eq. 3 gives the concentration of fluoride at the surface of an ice particle that has been growing for a time τ. Of course, at any point of time there are ice spherulites that have been growing since the first nuclei were formed, others that just started, and the range of τ is from one of these extremes to the other.

We seek the average concentration of solute $\langle C_0 \rangle$ seen by protein molecules as the spherical freezing interface passes by them. The concentration of hemeprotein is assumed to be constant, i.e., the same inside and outside of the ice spherulite (9), and the first average is over a spherulite which has grown (from $r_s = 0$) to final radius $r_{s,f}$.

$$\langle C \rangle_{0 \to r_{s,f}} = \left[\int_0^{r_{s,f}} C_s(4\pi r_s^2 dr_s)\right]/[4\pi(r_{s,f})^3/3] = C_0(1 + 3Rr_{s,f}/4D). \quad (4)$$

It is now necessary to average over the distribution in $r_{s,f}$ associated with the distribution in times t (after the start of the freezing process) when ice nuclei form. That is, $r_{s,f}$ in Eq. 4 is given by $R(t_0 - t)$, where t_0 is when the freezing process ends, and

$$\langle C_0 \rangle = \langle \langle C \rangle_{0 \to r_{s,f}} \rangle_{r_{s,f}} = C_0(1 + 3R\langle r_{s,f} \rangle/4D) \text{ with } \langle r_{s,f} \rangle = R\langle t_0 - t \rangle = R(t_0 - \langle t \rangle). \quad (5)$$

The probability that a spherulite starts at time t is proportional to the rate of formation, $V(t)v_n$, of ice nuclei. (Because the temperature is taken constant in this simple model, v_n is constant.) Thus

$$\langle t \rangle = \int_0^{t_0} V(t)v_n t dt / \int_0^{t_0} V(t)v_n dt \quad (6)$$

$$\text{and } \langle C_0 \rangle / C_0 = 1 + (3R^2/4D) \int_0^{t_0} V(r)v_n t dt / \int_0^{t_0} V(t)v_n dt. \quad (7)$$

$V(t)$ obeys the differential equation

$$d^4V(t)/dt^4 = -8\pi R^3 v_n V(t) \quad (8)$$

with solution

$$V(t) = V(0)\ \cos(ft/\sqrt{2})\cos h(ft/\sqrt{2}) \quad (9)$$

$$\text{where } f = (8\pi R^3 v_n)^{1/4}. \quad (10)$$

$$t_0 = \pi/\sqrt{2}f \quad (11)$$

is obtained by setting $V(t_0) = 0$. It follows that

$$\langle C_0\rangle/C_0 = 1 + 3R^2 t_0 \tanh(\pi/2)/2\pi D. \quad (12)$$

t_0 is the time required for the entire sample to freeze. The freezing of the sample solution in a polyethylene EPR sample cell can be monitored by a photodetector, as shown in Fig. 1, and t_0 is the period of time during which the optical transmission of the sample solution continuously decreases (see Fig. 9), corresponding to the time required for the whole sample to freeze.

As discussed at the end of the previous section, after Eq. 2, the intrinsic dissociation constant for the human metHb-fluoride complex at 250 K is estimated to be 12 ± 1 mM. One can then estimate the average local fluoride concentration from the mole fraction x of complex formed as measured by the EPR method. Thus

$$\langle C_0\rangle = [x/(1-x)]K_d. \quad (13)$$

Here x is measured at 77 K after rewarming and keeping sample at 250 K for 5 min, as shown in Figs. 6, 7, and 11.

The following formulas, obtainable from Eqs. 12, 10 and 11, and 6, enable one to use the available quantitative information to arrive successively at the rate of growth of the ice spherulites, their nucleation rate, and their time average radius, as functions of the ligand diffusion constant D.

$$R = [[(\langle C_0\rangle/C_0) - 1]D/0.45t_0]^{1/2} \quad (14)$$

$$v_n = 0.97 t_0^{-4} R^{-3} \quad (15)$$

$$\langle r_s\rangle = 0.58(R/v_n)^{1/4}. \quad (16)$$

Application of this formulation is demonstrated in Fig. 11 and Table 1.

B. Computer simulation of the freezing process

Because of the relatively large size of the EPR sample cell and the limited thermal conductivity of water and polyethylene, the presence of an external heat sink results in the formation of a temperature gradient between the center and outer surface of the sample cell during the coding process. Thus v_n, which is strongly dependent upon temperature, cannot be regarded as constant throughout the sample, an assumption of the simple kinetic model used above. A realistic treatment requires that the processes of heat flow, nucleation, and freezing be considered together, as in the computer simulation now to be described.

In this calculation, the sample cell is a polyethylene tube (ID 2.6 mm, wall = 0.4 mm, volume = 0.048 ml) filled with protein solution of low concentration (e.g. [Hb] = 0.247 mM in heme, [KF] = 1.18 mM, 33 mM phosphate, pH 6.3). The thermal conductivities of the sample solution, liquid and frozen, are taken to be the same as water (0.0055 $Wcm^{-1}K^{-1}$) and ice (0.022 $Wcm^{-1}K^{-1}$), respectively. The volume heat capacities of the sample are, analogously, taken as those of water (4.2 $Jcm^{-3}K^{-1}$) and ice, the temperature dependence of which is approximated by 0.159 + 0.00646T (T is the absolute temperature, K). The thermal conductivity and volume heat capacity of polyethylene are taken constant at 0.0035 $Wcm^{-1}K^{-1}$ and 2.0 $Jcm^{-3}K^{-1}$. (Thermal conductivities of various polyethylenes measured at temperatures between 100 and 300 K are in the range 0.002–0.005 $Wcm^{-1}K^{-1}$, generally greater at 200 than 300 K, then falling as the temperature is decreased below 200 K [33].) The thermal conductivity of the interface between the polyethylene cell wall and the cooling gas is taken as a variable. Only the latter parameter and the rate of ice growth (R) are permitted to vary with temperature, their values chosen to match the starting and completion times of freezing observed experimentally. The temperature gradient within the cylindrical sample during cooling is computed numerically as a function of time. One can view cooling as occurring in three phases, labeled as in Fig. 12 *a*: before nucleation, *A-B*; during freezing, *B-C*; and after freezing, beyond *C*. In approximating the cooling process, we divide the cylindrical volume between the outermost surface and the center into many thin layers. Then the temperature drop across each layer is calculated from the net rate of heat-flow from the layer and the heat capacity of the layer. As a layer supercools to the "critical" nucleation temperature (threshold for bulk ice formation), many ice nuclei start to form and grow, and a large amount of latent heat (of fusion) is released to the solution. There is also release of latent heat when ice, from the most recently frozen layer, grows into the layer undergoing freezing. When the rate of heat release exceeds the rate of heat conduction, the temperature of the layer undergoing freezing rises; as the temperature is pushed toward freezing point, nucleation stops. For the heat sink in the entire range utilized, 109–241 K, only 11–25% of the supercooled water in the outer layer will freeze before the temperature of the solution reaches 273 K.

To proceed with the calculation, an expression for the rate of heterogeneous nucleation in the protein solution

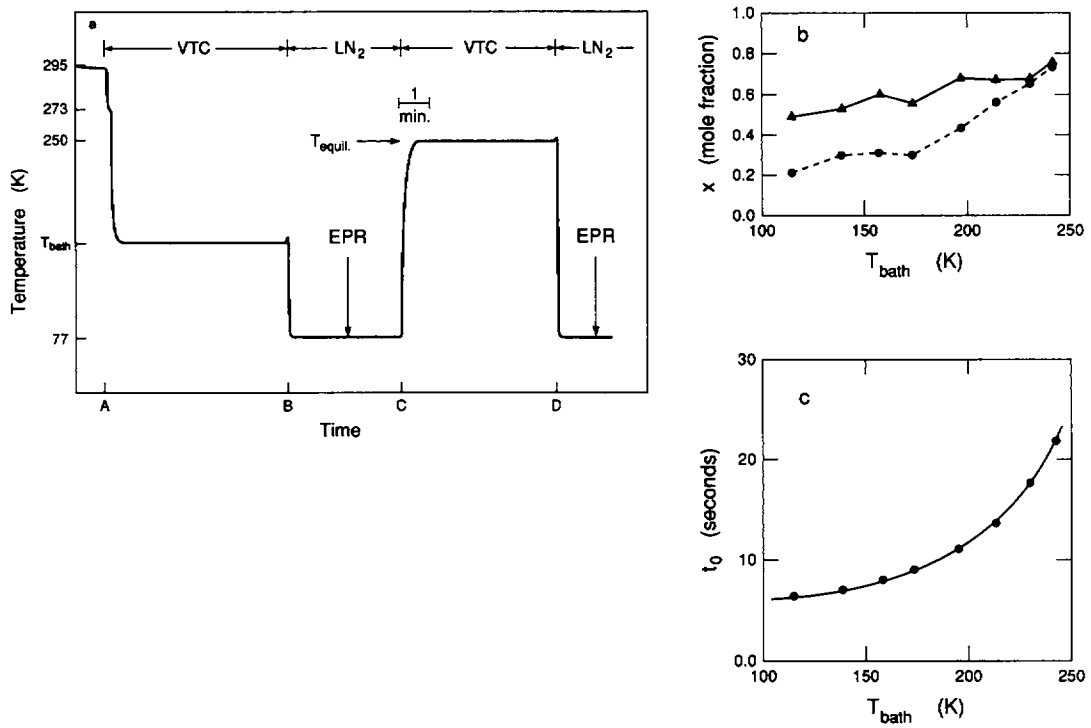

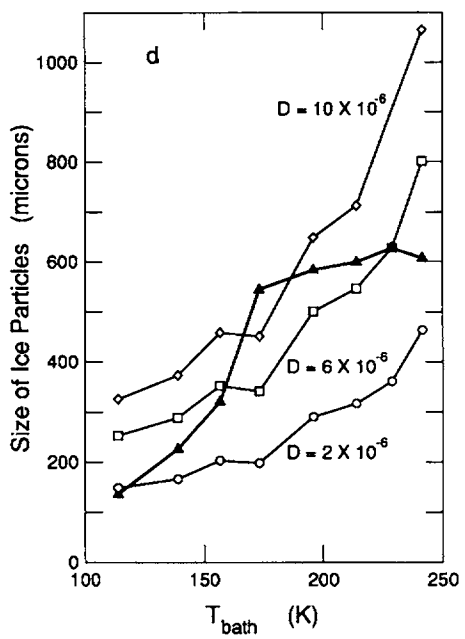

FIGURE 11 Experimental determination of mole fraction (x) of methemoglobin-fluoride complex, freezing time (t_0), and average ice spherulite radius ($\langle r_s \rangle$) as functions of freezing bath temperature (T_{bath}). (*a*) Protocol: at A the sample cell is inserted into the dewar of the variable temperature controller which is at temperature T_{bath} (measured with the thermocouple shown in Fig. 1). After 6 min at T_{bath}, the cell is immersed (*B*) in liquid nitrogen and the EPR spectrum measured (at 77 K). The cell is then warmed at T_{equil} for 5 min (*C-D*), after which it is plunged back into liquid nitrogen and the EPR spectrum measured again. (*b*) The mole fractions of fluoride complex, calculated from the EPR spectra measured before (●) and after (▲) the warming procedure, are shown as functions of T_{bath}. Sample solutions contained human methemoglobin, [heme] = 0.177 mM; in 33 mM phosphate buffer, pH 6.3, with [KF] = 0.59 mM. The EPR settings are the same as in Fig. 2, except that the power was set at 230 mW. The x- and y-axes are T_{bath} and mole fraction of fluoride complex, respectively. (*c*) t_0 plotted as a function of T_{bath}. The data for this figure is from Fig. 9. (*d*) The time average spherulite radius (r_s), calculated with Eq. 16 for several values of D (○, 2×10^{-6}; □, 6×10^{-6}; ◇, 10×10^{-6} cm^2/s), is plotted as a function T_{bath}. The time average length of the ice bodies $\langle \ell \rangle$ calculated by computer simulation of the freezing process, is also shown (▲) as a function of T_{bath}.

is required. The heterogeneous nucleation rate for ice crystals in an aqueous solution depends upon the surface characteristics and number of nucleation particles, information not available for the protein solutions. Therefore a parameterized nucleation rate equation, Eq. 17, is used here.

$$v_n(T) = F \exp\{-\gamma[\Delta G^*(T)]/RT\} \ (\text{cm}^{-3}\text{s}^{-1}), \qquad (17)$$

where the frequency factor F is of the order 10^{27} to 10^{30}, the parameter γ (with $0 < \gamma < 1$) expresses the deviation of the heterogeneous from the homogeneous nucleation rate ($\gamma = 1$) in pure water, and $\Delta G^*(T)$ is the free energy for a cluster of ice "germs" to grow to a critical radius ("embryo" formation, beyond which ice crystal growth proceeds) in pure water (13, 34). $\Delta G^*(T)$ has been calculated as a function of temperature from 273 to

TABLE 1 **Results of calculations of freezing process based upon two models**

	Simple kinetic model (for $D = 4 \times 10^{-6}\ cm^2/s$)				Computer simulation	
Bath	t_0	R	$\langle r_s \rangle$	R	$\langle \ell \rangle$	CONIF
K	s	$10^{-3}\ cm/s$	μm	$10^{-3}\ cm/s$	μm	$10^{-3}\ Wcm^{-1}K^{-1}$
113.8	6.3	5.6	205	18.0	134	.31
139.0	7.0	5.8	235	16.4	226	.31
157.0	8.0	6.2	288	13.7	320	.36
173.0	9.3	5.3	281	12.0	547	.37
195.8	10.9	6.4	410	10.7	586	.36
213.7	13.7	5.6	448	8.1	601	.38
228.5	17.5	5.0	508	6.1	629	.42
241	21.5	5.2	657	5.9	606	.25

233 K, in which range it drops from 1,700 to 54 $kJmol^{-1}K^{-1}$ (35). Because the critical temperature and the cooling time (point B, Fig. 12 *a*), for ice nucleation to start in the outer layer, depend upon the rate of nucleation, γ can be estimated by fitting the simulated cooling curves to the experimental ones (Figs. 9, 12, 13). A satisfactory match is obtained with γ in the range 0.04–0.05. Because, near the critical nucleation temperature, v_n increases by a factor of $\sim 10^7$ per degree of temperature drop, the critical nucleation temperature is only slightly dependent upon the rate of cooling. For $\gamma = 0.04$, simulations show a critical nucleation temperature of ~ 265.3 K when $T_{bath} = 241$ K, and less than a degree lower when $T_{bath} = 109$ K. As can be seen in Fig. 12 *a*, the outermost layer of the cylindrical solution sample reaches critical nucleation temperature first. The ice crystals start to grow from the outside toward the center of the cell.

The temperature decrease at each layer depends upon the difference between the rate of heat flow out and the rate of latent heat release, Eq. 18, from the growth of ice crystallites. For layer j with liquid phase volume V_j and density ρ_j

$$\text{rate of latent heat release} = -H_{f,water}\,(dV_j/dt)\rho_j, \quad (18)$$

where $H_{f,water}$ is the latent specific heat of fusion of water ($334\ Jg^{-1}$). The time dependence of the liquid volume is treated with Eqs. 9 and 10 (formation of new ice crystallites) together with propagation (at R cms^{-1}) of both the surface of crystallites already formed and the ice face of the most recently frozen layer (consolidation). These contributions are calculated at each step of time, the intervals ranging from 100 to 10 μs as the bath temperature is decreased from 241 to 109 K. Latent heat of fusion from ice growth increases the temperature and flows both ways, outward to the heat sink and inward to the inner layers of supercooled solution. The latter heat input inhibits nucleation in the inner solution. After nucleation and freezing of the outermost layer, subsequent ice growth in the next linear two-thirds of the sample takes place mainly by consolidation, heat being conducted to the sink through the outer ice then present. As the bath temperature is lowered, the number of ice nuclei (calculated for each layer during simulation of the freezing process) in the central region increases relative to outer region. Simulations (Figs. 12 and 13), which reproduce the salient features of the measured (with a thermocouple, Fig. 12, and optically, Fig. 9) cooling curves, also provide the time average length $\langle \ell \rangle$ of the ice bodies, each grown from one nucleus. This length, as a function of bath temperature, is presented both in Table 1 and in Fig. 11 *d*, where it can be compared with that from the simple kinetic model. Also given in Table 1 is the thermal conductivity (CONIF) of the polyethylene/nitrogen gas interface as a function of temperature. The values of the latter parameter, obtained from the simulations, do not differ greatly from those of nitrogen gas in the same range of temperature.

DISCUSSION

The binding of fluoride to heme proteins is pH dependent. At 5°C, in the pH range from 5.8 to 6.8, at an ionic strength of 0.05 M, the fractional increase in K_d for the reaction of fluoride with human methemoglobin is 0.24 per unit of pH (6). The question arises as to the influence upon fluoride complex formation of pH changes during freezing. Such changes in pH result from differing incorporation of buffer species into the solid phase, causing a shift in the ratio of basic to acid forms in the freezing solution phase (an expression of the phenomenon with which this paper deals). The apparent pH

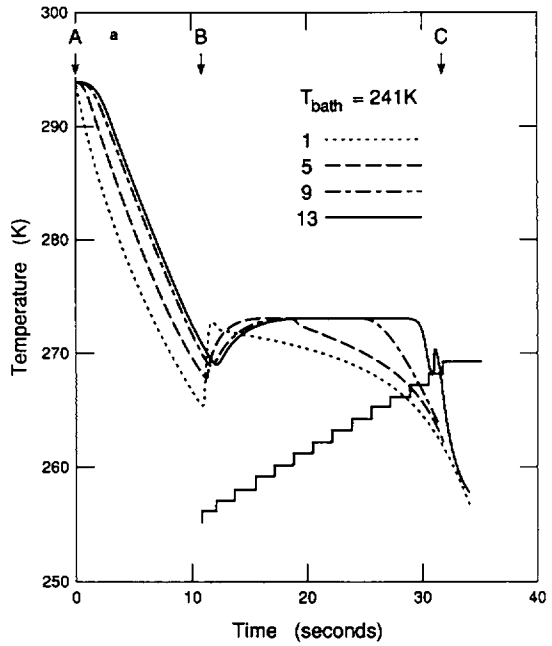

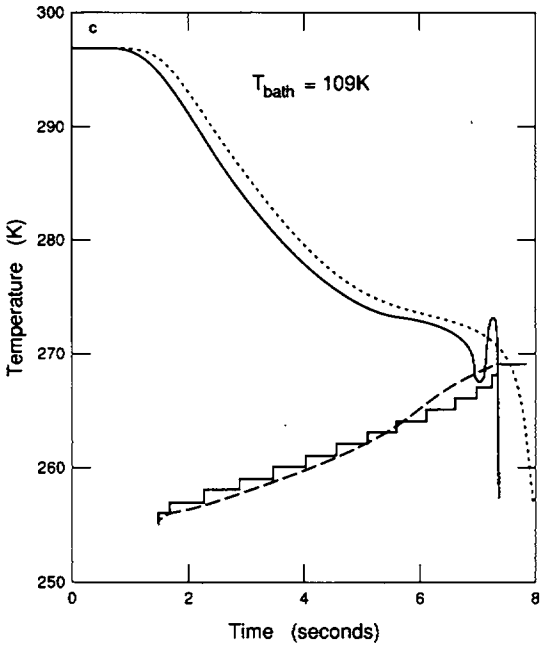

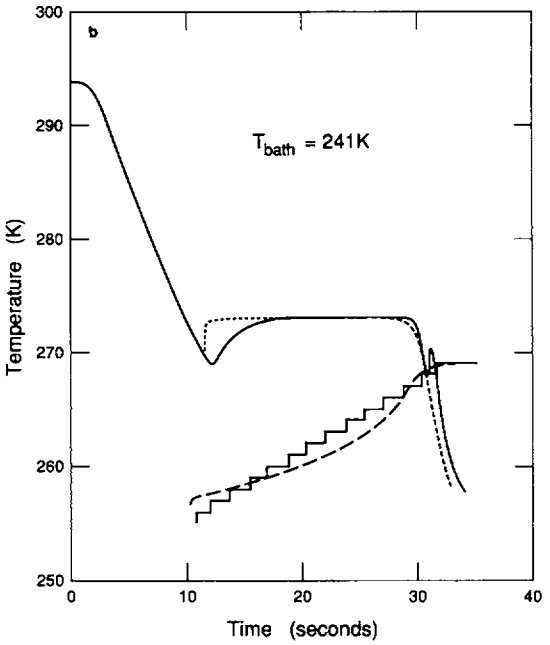

FIGURE 12 Simulated cooling curves of EPR sample (in polyethylene cell) in cold nitrogen bath. (*a*) T_{bath} = 241 K. The cylindrical sample volume is divided into 12 annular layers of equal thickness (0.1 mm), with a cylinder of radius 0.1 mm at the center. Simulated cooling curves are shown of (1) layer at outer surface, (5) fifth layer in, (9) ninth layer in, (13) at the center. The stepped function under the cooling curves describes the propagation of ice from the outer surface of the cylindrical sample toward the center; the length of each step represents the period of the time needed to complete the freezing process in the corresponding layer. (*b*) T_{bath} = 241 K. A comparison is shown of the calculated cooling curve at the center of the sample (*solid line*) with the experimental one (*dotted line*) measured by a thermocouple inserted in the center of the cell. Also shown are the calculated propagation of ice (*stepped function*) and the optically obtained data (*dashed line*), (Figs. 1 and 9); these two functions are normalized to the same final amplitude, but are not expected to have the same shape. (*c*) As in *b*, except T_{bath} = 109 K.

(from color of indicator added to solution) of an aqueous buffer can increase or decrease significantly when the solution is frozen, and such changes are suppressed by protein and glycerol (36, 37). The apparent pH of an approximately neutral solution of 0.1 M potassium phosphate decreases by 1.1 ± 0.3 when a tube containing it is immersed in liquid nitrogen; for sodium phosphate, the decrease is 1.9 ± 0.5 (36). With 4% (0.6 mM) bovine serum albumin present, freezing increases the apparent pH of the potassium phosphate by 0.1 ± 0.1 while for sodium phosphate the decrease is reduced to 0.3 ± 0.1. The effect of such freezing-induced pH changes cannot account for the dependence of K_{ad} upon protein and sucrose concentrations shown in Figs. 4 and 5. The question also arises as to the influence upon fluoride complex formation of changes in ionic strength during freezing. An increase in the ionic strengths of the solutions (which are on the acid side of the isoelectric pH of the proteins) in the experiment described in this paper would, on the basis of measurements (at room temperature) on related hemeprotein reactions (38), decrease the tightness of binding of fluoride; this effect

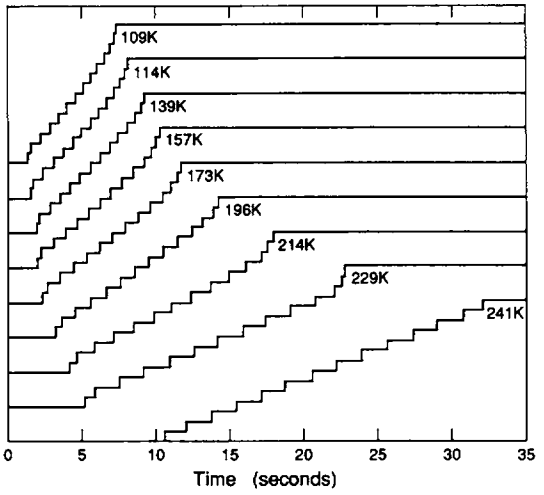

FIGURE 13 Simulated propagation of ice (stepped functions, as in Fig. 12) at various bath temperatures. The lengths of the steps enable one to see how the times for freezing successive layers change as the solid phase moves from the outer surface of the sample toward the center, and to compare the corresponding times at different bath temperatures. These functions are related, but not identical, to the experimental optical transmission curves shown in Fig. 9.

would be of opposite sign and significantly smaller in magnitude than the phenomenon reported here.

Proteins in solution and in crystals exhibit variability with respect to freezing-induced structural changes, damage, and disorder. Physical measurements show that, in general, the passage through freezing is continuous, with the protein parameters measured changing smoothly and monotonically. In some cases, interesting and as yet not understood phenomena have been observed; for example, there are complex changes in the magnetic susceptibility of horse aquo (39) and carp azide (40) aquomethemoglobins near the freezing point. Crystals of insulin (41), myoglobins (42–44), hemoglobins (45, 46), and cytochrome *c* (47) are little affected by freezing, although successive cycles of freezing and thawing of such crystals can produce measurable deterioration (48). The influence of having been frozen (with buffering under careful control) upon the activity of catalase has been studied as a function of enzyme concentration, rate of cooling, salt concentration, and concentration of cryoprotectants (49). Several factors, consistent with the experimental results and analysis reported in this paper, were found to be effective in protecting the catalase from freezing-induced loss of activity: high concentrations of protein and added cryoprotectants, low concentration of salt, rapid freezing, and choice of buffer system. There is an effect of anion concentration upon the low temperature EPR spectra of transferrin (50, 51). A subtle effect of protein concentration upon the structure of aquomethemoglobin at 77 K is evidenced by a change in the EPR lineshape of the $g = 6$ resonance; an even smaller change in lineshape is seen in aquometmyoglobin when its concentration is changed (Brill, A. S., unpublished results).

In this paper, a new method for investigating the ion-concentrating effect of the aqueous freezing process has been described. Titration of heme proteins with fluoride is followed by EPR spectroscopy, and the concentration of fluoride effective in producing complex formation with the iron estimated. With this technique, quantitative measures are obtained of the influences on effective fluoride concentration of the hemeproteins themselves (as a function of their concentration), of other solutes, and of the rate of cooling. A simple kinetic model is proposed, leading to a mathematical expression which relates the average size of ice spherulites to the time required for freezing (t_0), the diffusion constant for the ligand (D), and the ligand concentration ratio produced by freezing ($\langle C \rangle / C_0$). Estimates of the rates of ice growth (R) and nucleation (v_n) are also obtained. Qualitatively, solute redistribution (ligand concentration) increases with increasing size of the ice bodies. Quantitatively there are limitations in the formulation because of the simplified assumptions about protein and fluoride mobilities, and constant and uniform nucleation rate. The difference between the time course predicted by Eq. 9 and that which is observed, Fig. 9, and the calculated appreciable temperature gradient in the sample solution shown in Fig. 12 *a*, demonstrate that a more complex model, which includes heat transfer and latent heat generation, is necessary for a realistic simulation of the freezing process. Principles and results of such a computer simulation are presented. In Fig. 11 *d*, one sees that there is satisfactory (but not quantitative) agreement between the two models with regard to the dependence upon freezing bath temperature of the average dimensions of the ice bodies.

Within the limitations of the simple kinetic model, the results presented in Table 1 can be used to estimate the maximum concentration of fluoride to which the protein is exposed at each bath temperature. This greatest concentration occurs at the surface of ice particles that have been growing during the entire freezing process, a time t_0. The radius of such a particle, $r_{s,max} = Rt_0$, when used in Eq. 3 gives the maximum fluoride concentration at the interface, $C_{s,max}$, and the limiting freezing-induced concentration elevation ratio $C_{s,max}/C_0$. For the data of Table 1, including $D = 4 \times 10^{-6}$ cm^2/s, the latter ratio is readily calculated to be 50 for the sample frozen in the 113.8 K bath, increasing to 146 in the 241 K bath. In the experiments upon which Table 1 is based, C_0 (the homogeneous concentration of KF in the sample solutions as prepared at room temperature) was 0.59 mM.

The maximum fluoride concentrations are then estimated to be ~30 mM for the sample in the 113.8 K bath and ~86 mM in the 241 K bath. The solubility of KF in water at 265 K is 4.8 M, 56 times greater than 86 mM. (As derived from nuclear magnetic resonance measurements on the ternary system H_2O-KF-bovine serum albumin in the range of temperatures 238–208 K, the temperature dependence of the solubility of KF in the "nonfrozen" water is a linear extension of the dependence of the actual solubility of KF in water at temperatures between 282 and 252 K (53); at 208 K, the solubility of KF in the ternary system in ~1 M).

The effectiveness of a solute in inhibiting the freezing-induced concentration of fluoride depends upon its influence on the rates of ice nucleation (v_n) and growth (R). Recent research on one of the antifreeze polypeptides from fish suggests a structural mechanism whereby protein can interfere with the growth of ice (54). The extent of occurrence of such protein-ice interactions is not yet known, and a role for protein in ice nucleation remains to be confirmed or denied. Investigations exploring the influences of the size, composition, and charge of proteins and other molecules on v_n and R can be carried out with the new methods reported in this paper. Clearly the concentration of the species being added is an important experimental variable, but it can play upon more than one factor. Above some level of concentration, an additive such as sucrose (or glycerol or protein) will begin to slow the diffusion of fluoride, thereby increasing the average concentration of the ligand $\langle C_0 \rangle$ seen by the heme protein molecules; the latter change is in opposition to the result of the effects of the additive upon ice nucleation and growth rates.

Deeper insight into the freezing process, and new information about the influences of solute additives, bath temperatures for freezing and equilibrium, and sample cell heat transfer are provided by the research reported here. This new knowledge can be used to design more effective experiments when the observation of titrations and reaction intermediates at low temperatures is necessary. Furthermore, the estimation of average ice spherulite size by the quick and quantitative method described here can provide an efficient, practical means for evaluating conditions that minimize freezing damage. The results at hand call for additional basic and applied research along this line.

The support of the National Foundation under grant DMB-8517819 is acknowledged with appreciation.

Received for publication 2 May 1990 and in final form 15 October 1990.

REFERENCES

1. Keilin, D., and E. F. Hartree. 1951. Purification of horse-radish peroxidase and comparison of its properties with those of catalase and methaemoglobin. *Biochem. J.* 49:88–104.
2. Theorell, H., and A. Ehrenberg. 1951. Spectrophotometric, magnetic, and titrimetric studies on the heme-linked groups in myoglobin. *Acta Chem. Scand.* 5:823–848.
3. George, P. 1956. On the nature of hemoprotein reactions. *In* Currents in Biochemical Research. D. E. Greene, editor. Interscience Publishers, Inc., New York. 338–375.
4. Scheler, W., G. Schoffa, and F. Jung. 1957. Lichtabsorption und paramagnetische suszeptibilität bei derivaten des pferde- und chironomous-methämoglobins sowie des pferde-metmyoglobins. *Biochem. Z.* 329:232–246.
5. Havemann, R., and W. Haberditzl. 1958. Über die Beziehungen zwischen magnetischen, optischen und chemischen Eigenschaften von Hämoglobinderivaten. *Z. Physik. Chem. (Leipzig).* 290:135–161.
6. Anusiem, A. C., J. G. Beetlestone, and D. H. Irvine. 1968. Reactivity differences between haemoglobins. Part VIII. The thermodynamics of the reaction of human methaemoglobins A and C with fluoride, thiocyanate, and cyanide ions. An interpretation of enthalpy changes in terms of hydration. *J. Chem. Soc. (A).* 960–969.
7. Ross, R. T. 1965. Dipolar broadening of EPR spectra due to solvent segregation in frozen aqueous solutions. *J. Chem. Phys.* 42:3919–3922.
8. Pincock, R. E. 1969. Reactions in frozen systems. *Accounts Chem. Res.* 2:97–103.
9. Taborsky, G. 1970. Effect of freezing and thawing on the conformation of phosvitin. *J. Biol. Chem.* 245:1054–1062.
10. Taborsky, G. 1970. Solute redistribution in some multicomponent aqueous systems on freezing. *J. Biol. Chem.* 245:1063–1068.
11. Leigh, J. S. Jr., and G. H. Reed. 1971. Electron paramagnetic resonance studies in frozen aqueous solutions. Elimination of freezing artifacts. *J. Phys. Chem.* 75:1202–1204.
12. Taborsky, G. 1979. Protein alterations at low temperatures: an overview. *In* Proteins at Low Temperature. O. R. Fennema, editor. American Chemical Society, Wash., DC. 1–26.
13. Franks, F. 1985. Biophysics and Biochemistry at Low Temperatures. Cambridge University Press, Cambridge.
14. Lovelock, J. E. 1953. The haemolysis of human red blood cells by freezing and thawing. *Biochem. Biophys. Acta.* 11:28–36.
15. Pegg, D. E., and M. P. Diaper. 1988. On the mechanism of injury to slowly frozen erythrocytes. *Biophys. J.* 54:471–488.
16. Rebhun, L. I. 1972. Freeze-substitution and freeze-drying techniques in electron microscopy. *In* Electron Microscopical Techniques. M. A. Hayat, editor. Van Nostrand-Reinhold, New York. 2:3–49.
17. Luyet, B. 1960. On various phase transitions occurring in aqueous solutions at low temperatures. *Annu. NY Acad. Sci.* 85:549–569.
18. Kuntz, I. E. 1979. Properties of protein-water systems at subzero temperatures. *In* Proteins at Low Temperature. O. Fennema, editor. American Chemical Society, Wash., DC. 27–33.
19. Terwilliger, J. P., and S. F. Dizio. 1970. Salt rejection phenomena in the freezing of saline solutions. *Chem. Eng. Sci.* 25:1331–1349.
20. Drost-Hansen, W. 1967. The water-ice interface as seen from the liquid side. *J. Colloid Interface Sci.* 25:131–160.

21. Luyet, B., and G. Rapatz. 1958. Patterns of ice formation in some aqueous solutions. *Biodynamica.* 8:1–68.

22. Rapatz, G., and B. Luyet. 1966. Patterns of ice formation in aqueous solutions of glycerol. *Biodynamica.* 10:69–80.

23. Rapatz, G., and B. Luyet. 1972. Patterns of ice formation and rates of ice growth in gelatin solutions. *Biodynamica.* 11:117–123.

24. Rapatz, G., and B. Luyet. 1972. Patterns of ice formation in albumin solutions. *Biodynamics.* 11:125–136.

25. Brill, A. S., B. W. Castleman, and M. E. McKnight. 1976. Association of methanol and ethanol with heme proteins. *Biochemistry.* 15:2309–2316.

26. Austin, R. H., K. W. Beeson, L. Eisenstein, H. Frauenfelder, and I. C. Gunsalus. 1975. Dynamics of ligand binding to myoglobin. *Biochemistry.* 16:5355–5373.

27. Yang, A.-S., and A. S. Brill. 1989. Sub-freezing temperature jump study of the binding process of fluoride to heme proteins. *Biophys. J.* 55:558*a*. (Abstr.)

28. Lusena, C. V., and W. H. Cook. 1954. Ice propagation in systems of biological interest. II. Effect of solutes at rapid cooling rates. *Arch. Biochem. Biophys.* 50:243–251.

29. Lusena, C. V. 1955. Ice propagation in systems of biological interest. III. Effect of solutes on nucleation and growth of ice crystals. *Arch. Biochem. Biophys.* 51:277–284.

30. MacKenzie, A. P. 1977. Non-equilibrium freezing behaviour of aqueous systems. *Phil. Trans. Roy. Soc. B.* 278:167–189.

31. Pohl, R. G. 1954. Solute redistribution by recrystallization. *J. Chem. Phys.* 25:1170–1178.

32. Harrison, J. D., and W. A. Tilber. 1963. Controlled freezing of water. *In* Ice and Snow. W. D. Kingery, editor. MIT Press, Cambridge, MA. 215–225.

33. a) Hall, C. 1989. Polymer Materials. 2nd ed. John Wiley and Sons, New York. 93.
    b) Childs, G. E., L. J. Ericks, and R. L. Powell. 1973. Thermal Conductivity of Solids at Room Temperature and Below. U.S. Department of Commerce, National Bureau of Standards, Wash. DC. 535

34. Fletcher, N. H. 1970. The Chemical Physics of Ice. Cambridge University Press, Cambridge, MA. 73–103.

35. Dufour, L., and R. Defay. 1963. Thermodynamics of Clouds. Academic Press, New York. 165–181.

36. Williams-Smith, D. L., R. C. Bray, M. J. Barber, A. D. Tsopanakis, and S. P. Vincent. 1977. Changes in apparent pH on freezing aqueous buffer solutions and their relevance to biochemical electron-paramagnetic-resonance spectroscopy. *Biochem. J.* 167: 593–600.

37. Orii, Y., and M. Morita. 1977. Measurement of the pH of frozen buffer solutions by using pH indicators. *J. Biochem.* (*Tokyo*). 81:163–168.

38. Bettlestone, J. G., and D. H. Irvine. 1968. Reactivity differences between haemoglobins. Part VII. The effect of ionic strength on the affinity of methaemoglobins A and C for Azide Ion. A test of the dielectric cavity model for methaemoglobins. *J. Chem. Soc.* (*A*). 951–959.

39. Iizuka, T., and M. Kotani. 1969. Analysis of thermal equilibrium between high-spin and low-spin states in ferrihemoglobin complexes. *Biochim. Biophys. Acta.* 194:351–363.

40. Messana, C., M. Cerdonio, P. Shenkin, R. W. Noble, G. Fermi, R. N. Perutz, and M. F. Perutz. 1978. Influence of quaternary structure of the globin on thermal spin equilibria in different methemoglobin derivatives. *Biochemistry.* 17:3652–3662.

41. Brill, A. S., and J. H. Venable, Jr. 1968. The binding of transition metal ions in insulin crystals. *J. Mol. Biol.* 36:343–353.

42. Yonetani, T., and J. S. Leigh, Jr. 1971. Electromagnetic properties of hemoproteins. IV. Single crystal electron paramagnetic resonance spectroscopy of hemoproteins at ambient temperature. *J. Biol. Chem.* 246:4174–4177.

43. Scholes, C. P., A. Lapidot, R. Mascarenhas, T. Inubishi, R. A. Isaacson, and G. Feher. 1982. Electron nuclear double resonance (ENDOR) from heme and histidine nitrogens in single crystals of aquometmyoglobin. *J. Am. Chem. Soc.* 140:2724–2735.

44. Fiamingo, F. G., A. S. Brill, D. A. Hampton, and R. Thorkildsen. 1989. Energy distributions at the high-spin ferric sites in myoglobin crystals. *Biophys. J.* 55:67–77.

45. Hampton, D. A., and A. S. Brill. 1979. Crystalline state disorder and hyperfine component line widths in ferric hemoglobin chains. *Biophys. J.* 25:301–312.

46. Hori, H., M. Ikeda-Saito, and T. Yonetani. 1982. Ligand orientation of oxyproto- and oxy-mesocobalt porphyrin-substituted myoglobin by single crystal epr spectroscopy. *J. Biol. Chem.* 257:3636–3642.

47. Mailer, C., and C. P. S. Taylor. 1972. Electron paramagnetic resonance study of single crystals or horse heart ferricytochrome c at 4.2°K. *Can. J. Biochem.* 50:1048–1055.

48. Yonetani, T., and H. Schleyer. 1967. Electromagnetic properties of hemoproteins. I. Electron paramagnetic resonance absorptions of single crystals of ferrimyoglobin and cytochrome *c* peroxidase. *J. Biol. Chem.* 242:3919–3925.

49. Fishbein, W. N., and J. W. Winkert. 1979. Parameters of freezing damage to enzymes. *In* Proteins at Low Temperature. O. R. Fennema, editor. American Chemical Society, Washington, D.C. 55–82.

50. Price, E. M., and J. F. Gibson. 1972. Electron paramagnetic evidence for a distinction between the two iron-binding sites in transferrin and conalbumin. *J. Biol. Chem.* 247:8031–8035.

51. Yang, A.-S., and B. J. Gaffney. 1987. Determination of relative spin concentration in some high-spin proteins using E/D–distribution in electron paramagnetic resonance. *Biophys. J.* 51:55–67.

52. Muldrew, K., and L. E. McGann. 1990. Mechanisms of intracellular ice formation. *Biophys. J.* 57:525–532.

53. Ramirez, J. E., J. R. Cavanaugh, and J. M. Purcell. 1974. Nuclear magnetic studies of frozen aqueous solutions. *J. Phys. Chem.* 78:807–810.

54. Yang, D. S. C., M. Sax, A. Chakrabartty, and C. L. Hew. 1988. Crystal structure of an antifreeze polypeptide and its mechanistic implications. *Nature* (*Lond.*). 333:232–237.